Contents lists available at ScienceDirect

Optics Communications

Numerical errors of diffraction computing using plane wave spectrum decomposition

Tomasz Kozacki *

Institute of Micromechanics and Photonics, Warsaw University of Technology, Sw. A. Boboli 8, 02-525 Warsaw, Poland

ARTICLE INFO

ABSTRACT

In the paper the numerical determination of diffraction patterns using plane wave spectrum decomposition (PWS) is investigated. The simple formula for sampling selection for error-free numerical computation is proposed and its applicability is discussed. The usage of this formula presents practical difficulty for some diffraction problems due to required large memory load. A new multi-Fourier transform PWS (MPWS) method is elaborated which overcomes memory requirement of the PWS method. The performances of the PWS and MPWS methods are verified through extensive numerical simulations.

© 2008 Elsevier B.V. All rights reserved.

1. Introduction

In the development of optical technologies the need for more accurate optical models is constantly growing. To meet this demand the methods for diffraction field determination and their accuracy are extensively investigated. These methods are widely applied to solve problems of relation of optical fields between two separated planes. Digital holography [1], diffraction tomography [2], design of diffractive optical elements [3], and numerical refocusing [4,5] are the exemplary optical techniques utilizing such methods.

A computer aided analysis of general diffraction between two parallel planes based on the Rayleigh–Sommerfeld integral [6] involves two main approaches. The first one is based on a direct integration of the Rayleigh–Sommerfeld integral through discrete convolution of an optical field and the free space propagation impulse response. In the second approach an optical field is decomposed into plane waves and the propagation is computed using the angle dependent phase accommodation.

In this paper the plane wave spectrum decomposition (PWS) method is investigated. Such a decomposition is additionally used in the free-space beam propagation studies between arbitrarily oriented planes [7] and in problems of diffraction by micro optical elements [8–10]. We concentrate our study on the numerical errors of diffraction field determination between two parallel planes using plane wave spectrum. The errors of the PWS method were discussed by Shen et al. [11]. It was stated that the diffraction computing error depends on the size of a computation window and the general guidelines for the window size selection were given. To treat this issue in a more detailed way we utilized the spatial fre-

quency localization approach [12] to derive formula for the window size selection. For many practical cases of diffraction field determination the required window size grows and presents technical difficulty, necessary memory buffers for the algorithm are too large. This was the motivation for investigating a new algorithm without a need for such memory buffers. This algorithm is called the multi-Fourier transform PWS method (MPWS) and it is introduced in Section 4. Section 5 presents accuracy tests of the PWS and MPWS methods. In Appendix A the MPWS algorithm is derived.

2. Plane waves spectrum decomposition

Let us consider diffraction in a linear, homogenous and isotropic medium, where an optical field distribution is given as $u(x, y, 0)$, on the plane $z = 0$. It is known [13] that in the half plane $z > 0$ the propagation of an optical field using PWS at the output plane ($r = [x, y, z]$) can be expressed by

$$u(\mathbf{r}) = \left(\frac{1}{2\pi}\right)^2 \int_{-\infty}^{\infty} \int U^{z=0}(\mathbf{k}_t)\exp\{i\mathbf{k} \cdot \mathbf{r}\} \, d\mathbf{k}_t \tag{1}$$

using plane wave spectrum decomposition at input plane ($r = [x, y, 0]$)

$$U^{z=0}(\mathbf{k}_t) = \int_{-\infty}^{\infty} \int u(\mathbf{r}_t, 0)\exp\{-i\mathbf{k}_t \cdot \mathbf{r}_t\}d\mathbf{r}_t, \tag{2}$$

where corresponding vectors are given by

$$\mathbf{r}_t = x\hat{e}_x + y\hat{e}_y,$$
$$\mathbf{k} = \mathbf{k}_t + k_z\hat{e}_z, \mathbf{k}_t = k_x\hat{e}_x + k_y\hat{e}_y,$$
$$k_z = \begin{cases} \sqrt{k^2 - \mathbf{k}_t \cdot \mathbf{k}_t} & \text{if } \mathbf{k}_t \cdot \mathbf{k}_t \leqslant k^2, \\ +i\sqrt{\mathbf{k}_t \cdot \mathbf{k}_t - k^2} & \text{if } \mathbf{k}_t \cdot \mathbf{k}_t > k^2 \end{cases}.$$

* Tel.: +48 224328635.
  E-mail address: t.kozacki@mchtr.pw.edu.pl

The $\hat{e}_{x,y,z}$ are the unit vectors and the dot in Eqs (1) and (3) denotes the vector scalar product.

Eq. (2) can be expressed in the form relating the Fourier spectra of an optical field at the output [$\mathbf{r_t}$, z] and input [$\mathbf{r_t}$, 0] planes, i.e.,

$$\tilde{u}(\mathbf{f}_t, z) = \tilde{u}(\mathbf{f}_t, 0)H(\mathbf{f}_t), \qquad (3)$$

where

$$H(\mathbf{f}_t) = \begin{cases} \exp\{ikz\sqrt{1 - \lambda^2\mathbf{f}_t \cdot \mathbf{f}_t}\} & \text{if } \mathbf{f}_t \cdot \mathbf{f}_t \leqslant \lambda^{-2} \\ \exp\{-kz\sqrt{\lambda^2\mathbf{f}_t \cdot \mathbf{f}_t - 1}\} & \text{if } \mathbf{f}_t \cdot \mathbf{f}_t > \lambda^{-2} \end{cases}$$

is the kernel of the PWS method.

The tilde denotes Fourier Transform $\tilde{g}(\mathbf{f}_t) = \int_{-\infty}^{\infty} g(\mathbf{r}_t)$ $\exp\{-2\pi i \mathbf{r}_t \cdot \mathbf{f}_t\}d\mathbf{r}_t$ and the Fourier frequency vector obeys relation $\mathbf{f}_t = [\cos(\alpha)/\lambda, \cos(\beta)/\lambda]$, where α, β are x, y directional cosines of the wave vector $\mathbf{k}$, respectively.

Eq. (3) is the essential part of the PWS algorithm where the optical field at the output plane $u(\mathbf{r_t}, z)$ is simply the Fourier transform of $\tilde{u}(\mathbf{f}_t, z)$.

3. Sampling error in PWS computation

The algorithm basing on Eq. (3) will produce precise discrete optical fields $u(\mathbf{r_t}, z)$ only if both $\tilde{u}(\mathbf{f}_t, z)$ and $H(\mathbf{f}_t)$ are band limited according to the Nyquist sampling theorem. In this Section the sampling of the PWS kernel employing spatial frequency localization is investigated. The evanescent fields are not considered. An improper sampling of a phase part of the PWS kernel is a major source of the PWS algorithm error. For simplicity of the presentation the analysis is performed in one dimension, the received result is readily applicable to the two dimensional case.

The phase part of the PWS kernel is a phase function with a constant amplitude containing high frequency information. To be properly sampled the phase increase of the PWS kernel between two consecutive samples can not exceed π.

In order to find necessary conditions of PWS kernel sampling we utilize local spatial frequency in the Fourier domain and we define spatial frequency position

$$x_{lf} = \frac{1}{2\pi} \frac{\partial(ARG[H(f)])}{df} = \frac{-\lambda z f}{\sqrt{1 - \lambda^2 f^2}}. \qquad (4)$$

The spatial frequency position associates particular frequency regions with spatial position. For small frequencies the distribution of spatial frequency localization grows linear, then diverges at frequency λ^{-1}.

The PWS algorithm configuration using Eq. (4) is presented in Fig. 1. It is required that, the spatial frequency position x_{lf} can not exceed dimensions of computational aperture $N_x\Delta_x/2$ i.e.,

$$|x_{lf}| = \left| \frac{-\lambda z f}{\sqrt{1 - \lambda^2 f^2}} \right| \leqslant \frac{N_x\Delta_x}{2}. \qquad (5)$$

For limiting case we introduce $f_{viol.}$, giving band limitation for computational algorithm:

$$f_{viol.} = \lambda^{-1}\left(1 + \frac{4z^2}{(N_x\Delta_x)^2}\right)^{-1/2}. \qquad (6)$$

In the numerical example presented in Fig. 1 the angular spectrum of the object wave is band limited to the Nyquist frequency, but the PWS kernel sampling condition is violated. At the object plane wave spectrum, the spatial frequencies higher then f_{viol} (viol. waves) will be multiplied by improperly sampled PWS kernel. At frequency f_{viol} the x_{lf} equals to the inverse of two frequency samples [$\Delta_{fx} = (N_x\Delta_x)^{-1}$]. Therefore, higher frequencies then f_{viol} cause
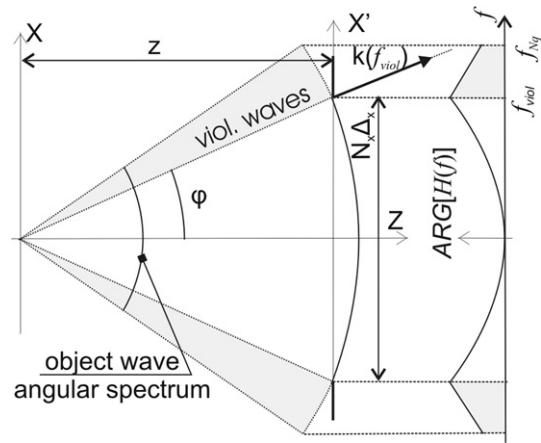
Fig. 1. PWS algorithm configuration visualization; the visualization is presented in both spatial (propagation field) and spatial frequency (phase of the kernel) domains; X-object plane, X′-propagation plane.

aliasing in the PWS kernel and PWS algorithm produces inaccurate results.

Above derivation can be visualized with experimental example, where the Nyquist frequency f_{Nq} corresponds to the limiting plane wave of the object spectrum and the computational aperture to the aperture at propagation plane. In this case the rays representing the plane wave originating from object centre with angle larger then

$$\varphi = \tan^{-1}\left(\frac{N_x\Delta_x}{2z}\right) = \tan^{-1}\left(\frac{\lambda f_{viol}}{\sqrt{1 - \lambda^2 f^2}}\right) \qquad (7)$$

will hit rim of the aperture. Additionally with increasing distance z the angular dimension of the aperture is smaller and the violating waves region grows.

The condition (6) gives the means of the PWS algorithm configuration, i.e., the adjustment of sampling parameters in order to avoid the PWS kernel aliasing. In practice, for analytically given optical distribution at the input plane, the sampling is chosen according to Eq. (6), whereas for an optical signal given by discrete samples, the condition (6) can be fulfilled through the signal data extension, e.g. signal zero padding.

To visualize numerical errors we chose discrete representation of the point source as an object and we test its propagation. Such an artificial exemplary object distribution has constant Fourier spectrum, so only propagation errors related to PWS kernel will be visualized. In Fig. 2 the difference between theoretical and
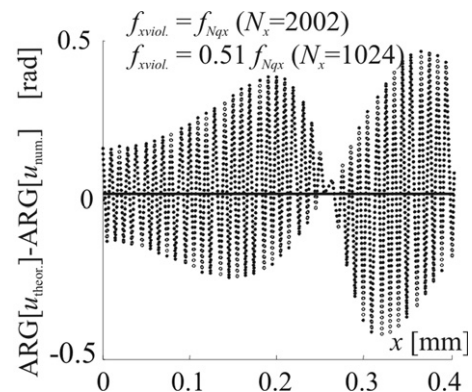
Fig. 2. Spatial error distribution of the phase computed for the point object and parameters z = 100 mm, λ = 0.5 μm, Δ_x = 5 μm.
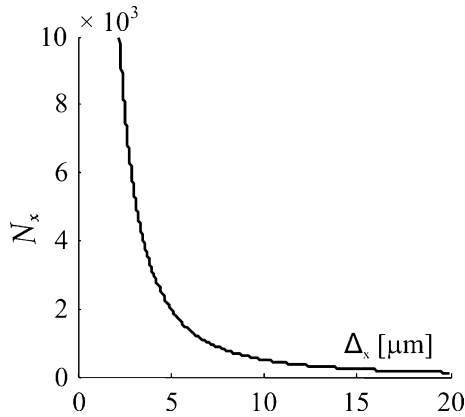
Fig. 3. The signal dimension N_x as a function of sample size $\varDelta_x$ for $z = 100$ mm, $\lambda = 0.5$ μm.

computed phase distributions for a point source is presented. The longitudinal distance between the source and diffraction plane is $z = 100$ mm. There are two distributions. One of the distributions was received by the propagation algorithm with the sampling condition $f_{xviol.} = f_{Nqx}$. The second distribution is obtained with violation of the sampling condition $f_{xviol.} = 0.51\, f_{Nqx}$.

Condition (6) can be cast to the form

$$N_x \geqslant \frac{2\lambda z}{\varDelta_x \sqrt{4\varDelta_x^2 - \lambda^2}} \tag{8}$$

showing the necessary signal dimensions for the PWS computational algorithm. In Fig. 3 the signal dimension is plotted as a function of sample size for an exemplary propagation distance. The PWS algorithm will produce correct results for the signal dimensions above the line only. For example at $\varDelta_x = 2.24$ μm the signal dimension grows rapidly ($N_x > 10000$) giving practical difficulty for the PWS algorithm configuration. For $N_x = 10000$ the algorithm uses 3.2 GB memory buffers.

4. Multi-Fourier transforms PWS method

In the preceding Section the necessity of the signal data extension was presented. It was shown that for some practical simulation cases such an extension can present practical difficulty due to large memory requirements. This was the motivation of the implementation of the zero padding algorithm where the use of such large memory buffers is not necessary. This algorithm we will call as the multi-Fourier transform PWS method (MPWS). The basic idea of the algorithm is the application of signal zero padding through multiple computation of modified PWS algorithms without enlarging of memory buffers. Detailed algorithm derivation is presented in Appendix A.

Consider input signal u_i of size $N \times N$. Let extend such a signal through zero padding by integer multiple A:

$$u_{ie}[n_x, n_y] = \begin{cases} u_i[n_x, n_y] \text{ if } 0 \leqslant n_x < N, \ 0 \leqslant n_y < N \\ 0 \quad \text{otherwise} \end{cases}, \tag{9}$$

where $n_x \in \langle 0 : N_e - 1 \rangle$, $n_y \in \langle 0 : N_e - 1 \rangle$ and $N_e = AN$ is the dimension of the extended array and A is the integer number.

Discrete Fourier spectrum of such a data array (size $AN \times AN$) can be represented by A^2 data arrays of size $N \times N$:

$$\tilde{u}_{ie}^{(\alpha,\beta)}[p,q] = \sum_{m=0}^{N-1} \sum_{n=0}^{N-1} u_i[n,m] \exp\left\{-2\pi i \frac{n\alpha + m\beta}{N_e}\right\}$$
$$\times \exp\left\{-2\pi i \frac{np + mq}{N}\right\}, \tag{10}$$

where α, β are integers in the range: $0 \leqslant \alpha < A$ and $0 \leqslant \beta < A$.

Therefore the DFT of the extended input array can be split into A^2 submatrixes marked by α and β. Each submatrix can be computed from DFT of input array u_i modified by the phase function of α and β. The submatrixes are shifted in frequency space by $\alpha/AN\varDelta_x$ and $\beta/AN\varDelta_x$, respectively.

Substituting Eq. (10) into Eq. (3) gives final formula for the optical field u_o at the output plane z:

$$u_o[n,m] = N_e^{-2} \sum_{\beta=0}^{A-1} \sum_{\alpha=0}^{A-1} \left(\begin{array}{l} \sum_{q=0}^{N-1} \sum_{p=0}^{N-1} \tilde{u}_{ie}^{(\alpha,\beta)}[p,q] H[p + \alpha A^{-1}, q + \beta A^{-1}] \\ \times \exp\left\{2\pi i \frac{np+mq}{N}\right\} \exp\left\{2\pi i \frac{n\alpha+m\beta}{N_e}\right\} \end{array} \right), \tag{11}$$

where array H stores coefficients of the PWS kernel swapped in the DFT specific manner:

$$H[u,v] = \begin{cases} \exp\{2\pi i z \varDelta_f \sqrt{\varDelta_f^{-2} \lambda^{-2} - u^2 - v^2}\} \\ \quad \text{for } 0 \leqslant u, \quad v < \frac{N}{2} - 1 \\ \exp\{2\pi i z \varDelta_f \sqrt{\lambda^{-2} \varDelta_f^{-2} - (u-N)^2 - v^2}\} \\ \quad \text{for } \frac{N}{2} \leqslant u < N - 1, \quad 0 \leqslant v < \frac{N}{2} - 1 \\ \exp\{2\pi i z \varDelta_f \sqrt{\varDelta_f^{-2} \lambda^{-2} - u^2 - (v-N)^2}\} \\ \quad \text{for } 0 \leqslant u < \frac{N}{2} - 1, \frac{N}{2} \leqslant \quad v < N - 1 \\ \exp\{2\pi i z \varDelta_f \sqrt{\varDelta_f^{-2} \lambda^{-2} - (u-N)^2 - (v-N)^2}\} \\ \quad \text{for } \frac{N}{2} \leqslant u, \quad v < N - 1 \end{cases}$$

$\varDelta_f = (N\varDelta_x)^{-1}$.

The formula is the base equation of the MPWS algorithm and allows to compute free space propagation of the input optical signal u_i through a distance z.

The MPWS algorithm can be reconfigured to padding with arbitrary complex constant A_0. Such a reconfiguration is accomplished with simple arithmetic operations:

– step 1: subtraction of constant A_0 from input optical field,
– step 2: propagation using MPWS algorithm with zero padding,
– step 3: addition of the constant $A_0\exp\{ikz\}$.

The MPWS algorithm produces the same result as the PWS method with zero padding data extension applied. Let us compare computation load of the PWS and MPWS algorithms with data zero padding. For the PWS method application of two DFT algorithms of data arrays of size $AN \times AN$ is required while for the MPWS method $2A^2$ DFT of data arrays $N \times N$ are necessary.

5. Accuracy test

This Section presents numerical study of the precision of the PWS and MPWS algorithms. First we assess the accuracy of algorithms by comparison with known diffraction solution. Then numerically obtained diffraction results with sampling according to condition (6) are explored.

Consider the diffraction problem where a circular aperture is illuminated by plane wave with wave vector normal to the aperture plane. For such a geometry the optical field distribution at the optical axis is known [14]. In Fig. 4 the amplitude of diffracted optical field along the axis is presented. Theoretical results and numerical values obtained with PWS (signal size 1024×1024) and MPWS methods ($N = 1024$) are given. The discrepancy between numerically computed amplitude with the PWS method and the theoretical solution appears for large propagation
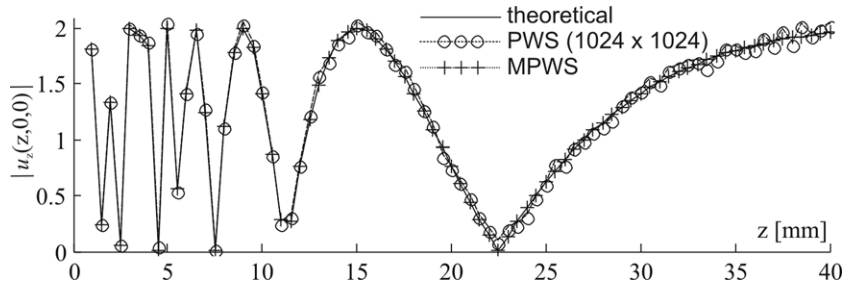
Fig. 4. On-axis amplitude variation received in the case of diffraction of a plane wave by circular aperture of radius 150 μm (Δ_x = 1 μm, wavelength 0.5 μm).
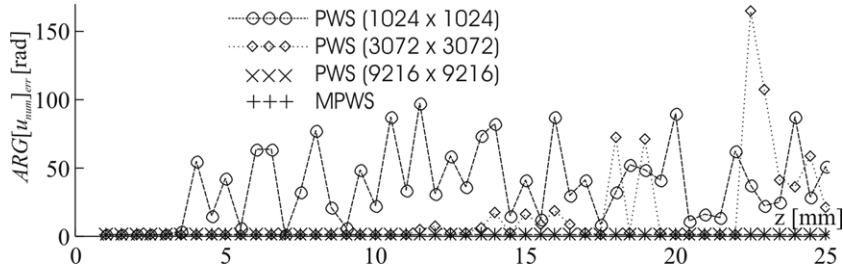
Fig. 5. The integrated phase error obtained for point source as a function of propagation distance for the PWS and MPWS methods (Δ_x = 1 μm, wavelength 0.5 μm).
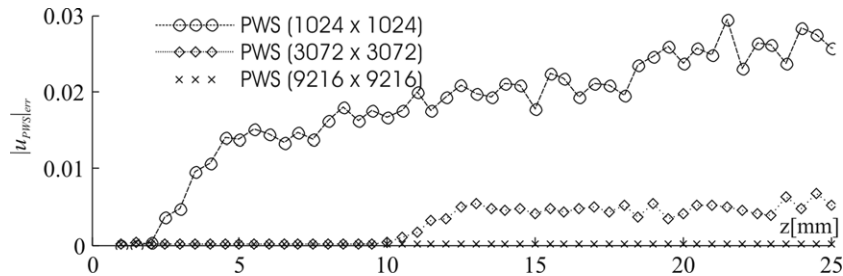
Fig. 6. The phase error obtained for diffraction by a circular aperture for the PWS and MPWS methods (Δ_x = 1 μm, wavelength 0.5 μm).

distances. The MPWS algorithm gives results with a good agreement with theoretical ones.

In the next numerical test a study of the impulse response is considered. The phase distribution $ARG[u_{num.}]$ at various propagation distances is calculated numerically with the PWS and MPWS methods for a point source. The integrated phase error resulting from comparison of the numerical results with the theoretically obtained phase $ARG[u_{thoer.}]$ was estimated via equation

$$ARG[u_{num.}]_{err} = \left[\frac{1}{N} \sum_{|\mathbf{r_t}|<r_0} [ARG[u_{theor.}(z, \mathbf{r_t})] - ARG[u_{num.}(z, \mathbf{r_t})]]^2 \right]^{1/2},$$ (12)

where r_0 = 0.25 mm and N is a number of considered numerical values. The phase errors are presented in Fig. 5. The errors computed for the PWS method for three array dimensions: 1024 × 1024, 3072 × 3072, and 9216 × 9216 are included. It is clear that the PWS for the largest matrix and the MPWS (N = 1024) algorithms give error-free phase distributions only at all considered propagation distances. The final test considers again the diffraction problem with circular aperture illuminated by plane wave normal to the aperture plane. For such a geometry the diffracted field was computed using PWS ($|u_{PWS}(z, \mathbf{r_t})|$, array dimensions 1024 × 1024, 3072 × 3072, and 9216 × 9216) and MPWS ($|u_{MPWS}(z, \mathbf{r_t})|$, N = 1024) methods. For various distances the integrated deviation

between amplitudes obtained with the PWS and MPWS methods were computed via equation

$$|u_{PWS}|_{err} = \left[\frac{1}{N} \sum_{|\mathbf{r_t}|<r_0} [|u_{MPWS}(z, \mathbf{r_t})| - |u_{PWS}(z, \mathbf{r_t})|]^2 \right]^{1/2}$$ (13)

with r_0 = 0.25 mm. The results $|u(z, \mathbf{r_t})|_{err}$ are plotted in Fig. 6 giving equivalent conclusions to these discussed above. Namely the diffracted field can be obtained precisely using the PWS method with sampling according to Eq. (6) or the MPWS method.

6. Conclusions

In the paper we undertook the study of numerical errors of diffraction computing between two parallel planes using the plane wave spectrum decomposition (PWS). The error depends on the selection of sampling parameters. Utilizing the spatial frequency localization this feature was investigated and the simple formula was given. It was shown that in order to produce accurate results for some diffraction computation cases a significant data extension is necessary. Such a data extension can present practical difficulty due to the required memory load. Therefore a modified method (MPWS) of computing the plane wave spectrum without necessity of data extension was presented. Simulation results have shown that both the PWS and MPWS methods provides accurate diffraction field when the correct sampling is applied.

Appendix A. MPWS algorithm derivation

In Section 3 the necessity of signal extension for large propagation distances was presented. For numerically given signal the Fourier spectrum sampling rate is determined by signal dimensions, but for same propagation distances can be to coarse. Therefore we apply signal data extension through zero padding. This technique is frequently used in signal processing to enhance signal resolution [15].

Consider 1D object data u_i of length N sampled with interval Δ. The plane wave spectrum u_o at distance z is given by

$$u_o(n\Delta) = N^{-1} \sum_{p=0}^{N-1} \tilde{u}_i(p\Delta_{\mathrm{f}}) H(p\Delta_{\mathrm{f}}) \exp\{2\pi i n p / N\}, \tag{A1}$$

where $\Delta_f = (N\Delta)^{-1}$.

In order to decrease sampling rate of input signal in Fourier domain we apply 1D zero padding according to Eq. (6) giving extended input signal u_{ie} of size $N_e = AN$ with plane wave spectrum

$$u_o(n\Delta) = N_e^{-1} \sum_{\alpha=0}^{A-1} \sum_{p=0}^{N-1} \tilde{u}_{ie}(p\Delta_{\mathrm{f}} + \alpha\Delta_{fe}) H$$
$$\times (p\Delta_{\mathrm{f}} + \alpha\Delta_{fe}) \exp\left\{\frac{2\pi i n p}{N}\right\} \exp\left\{\frac{2\pi i n \alpha}{N_e}\right\}, \tag{A2}$$

where $\Delta_{fe} = (N_e\Delta)^{-1}$.

The algorithm based on above equation would be inefficient, the extended input matrix is processed. For algorithm optimization the spectrum of object extended signal have to be split into A frequency subsignals shifted in frequency space:

$$\tilde{u}_{ie}(p\Delta_{\mathrm{f}} + \alpha\Delta_{fe}) = \sum_{n_e=1}^{N_e} u_{ie}(n_e\Delta) \exp\left\{-\frac{2\pi i n_e(Ap + \alpha)}{N_e}\right\}$$
$$= \sum_{n=1}^{N} u_i(n\Delta) \exp\left\{-\frac{2\pi i n p}{N}\right\} \exp\left\{-\frac{2\pi i \alpha n}{N_e}\right\}. \tag{A3}$$

Application of Eq. (A3) in Eq. (A2) gives final formula for 1D MPWS algorithm, where input signal without extension is processed:

$$u_o(n\Delta) = N_e^{-1} \sum_{\alpha=0}^{A-1} \sum_{p=0}^{N-1} \tilde{u}_{ie}(p\Delta_{\mathrm{f}} + \alpha\Delta_{fe}) H(p\Delta_{\mathrm{f}}$$
$$+ \alpha\Delta_{fe}) \exp\left\{\frac{2\pi i n p}{N}\right\} \exp\left\{\frac{2\pi i n \alpha}{N_e}\right\}. \tag{A4}$$

References

[1] L.P. Yaroslavskii, N.S. Merzlyakov, Methods of Digital Holography, Consultants Bureau, 1980.
[2] A.J. Devaney, Ultrason. Imaging. 4 (1982) 336.
[3] J.R. Fienup, Appl. Opt. 21 (15) (1982) 2758.
[4] F. Dubois, L. Joannes, J.-C. Legros, App. Opt. 38 (1999) 7085.
[5] T. Kozacki, M. Kujawinska, P. Kniazewski, Optoelectronics Review 15 (2007) 102.
[6] M. Born, E. Wolf, Principles of Optics, seventh ed., Cambridge University Press, Cambridge, 1999.
[7] N. Delen, B. Hooker, J. Opt. Soc. Am. A 15 (1998) 857.
[8] N. Lindlein, J. Opt. A: Pure Appl. Opt. 4 (2002) S1.
[9] A. Rohrbach, W. Singer, J. Opt. Soc. Am. A 15 (1998) 2651.
[10] K.H. Brenner, W. Singer, Appl. Opt. 32 (1993) 4984.
[11] F. Shen, A. Wang, Appl. Opt. 45 (2006) 1102.
[12] J.W. Goodman, Introduction to Fourier Optics, second ed., McGraw-Hill, 1996.
[13] J.J. Stamnes, Waves in Focal Regions, Hilger, Bristol, 1986.
[14] A. Dubra, J.A. Ferrari, Am. J. Phys. 67 (1999) 87.
[15] J.C. Santamarina, D. Fratta, Discrete Signals and Inverse Problems: An Introduction for Engineers and Scientists, John Wiley & Sons, 2005.